Controlling laser-induced magnetization reversal dynamics in a rare-earth iron garnet across the magnetization compensation point

Marwan Deb,[1,*] Pierre Molho,[2,3] Bernard Barbara,[2,3] and Jean-Yves Bigot[1,†]

[1]*Institut de Physique et Chimie des Matériaux de Strasbourg, UMR 7504, CNRS, Université de Strasbourg,
Boîte Postale 43, 23 rue du Loess, 67034 Strasbourg Cedex 02, France*
[2]*CNRS, Institut Néel, F-38042 Grenoble, France*
[3]*Université Grenoble Alpes, Institut Néel, F-38042 Grenoble, France*

In this work we explore the ultrafast magnetization dynamics induced by femtosecond laser pulses in a doped film of gadolinium iron garnet over a broad temperature range including the magnetization compensation point T_M. By exciting the phonon-assisted $^6S \rightarrow {}^4G$ and $^6S \rightarrow {}^4P$ electronic d-d transitions simultaneously by one- and two-photon absorption processes, we find out that the transfer of heat energy from the lattice to the spin has, at a temperature slightly below T_M, a large influence on the magnetization dynamics. In particular, we show that the speed and the amplitude of the magnetization dynamics can be strongly increased when increasing either the external magnetic field or the laser energy density. The obtained results are explained by a magnetization reversal process across T_M. Furthermore, we find that the dynamics has unusual characteristics which can be understood by considering the weak spin-phonon coupling in magnetic garnets. These results open new perspectives for controlling the magnetic state of magnetic dielectrics using an ultrashort optically induced heat pulse.

I. INTRODUCTION

Ultrafast magnetization dynamics driven by femtosecond laser pulses or "femtomagnetism" [1,2] is an active and rapidly expanding field of modern condensed matter physics since the discovery of the subpicosecond demagnetization of Ni films following excitation by a 60-fs laser pulse [3]. Many important phenomena induced by femtosecond laser pulse in magnetic materials have been demonstrated, such as a change of magnetic anisotropy [4], the generation of spin waves [5,6], all optical magnetization switching [7,8], ultrafast magnetic phase transitions [9–11], and the production of ultrashort spin-polarized current pulse [12,13]. These results promise impactful industrial applications in various areas including the magnetic storage and the control of spintronic devices. They also provide rich opportunities to progress in the understanding of fundamental issues related to the interaction of light with magnetic materials. One major issue is the effect of the energy transfer between the laser field and the different degree of freedom (charge, spins, lattice, and orbital and spin momenta) on the ultrafast magnetization dynamics. Another important issue is the mechanisms by which the light can directly affect the spins [14].

Despite the large variety of physical phenomena reported in the field of femtomagnetism, the different approaches used to manipulate magnetism by light can be classified into two main categories. The first is based on induced changes of the magnetic properties due to heating effects. Such heating results from the laser energy absorbed by the magnetic material and

it has been found to be essential for obtaining an ultrafast demagnetization [3] or an all-optical magnetization switching [15,16]. It also induces a subpicosecond magnetization reversal dynamics across the compensation temperature of rare-earth transition-metal metallic ferrimagnets, which can be controlled by the external magnetic field and the pump energy density [17–19]. The study of this reversal dynamics in GdFeCo using x-ray circular dichroism reveals a different dynamics of Gd and FeCo sublattices, which leads to a transient ferromagneticlike state [19]. This phenomenon was suggested to be at the origin of the single-shot all-optical magnetization switching in GdFeCo. The second category includes nonthermal mechanisms, inducing optical control of the magnetization such as the inverse Faraday [6,20] and Cotton-Mouton effects [21], which are needed, for example, for generating spin waves and manipulating their properties with the help of the polarization of light. In magnetic dielectric materials, most investigations of light-induced magnetization dynamics are focused on manipulating the magnetic resonance modes using nonthermal effects [6,21–31]. On the other hand, there are only few studies addressing the effect of ultrafast heating on the magnetization dynamics [32–34]. In particular, it was recently reported that a pure heating can induce an ultrafast spin-reorientation transition in some rare-earth orthoferrites [32,33]. An important question in this context is the possibility of taking advantage of such heating to trigger a magnetization reversal dynamics. Furthermore, studying the heating process in other classes of magnetic dielectrics like the iron garnets is very important to clarify how the difference in the electronic structures and the coupling between the spins and lattice can affects the ultrafast magnetic phenomena.

In the present work we experimentally explore the laser-induced ultrafast magnetization dynamics in a rare-earth iron

*Corresponding author: marwan.deb@ipcms.unistra.fr
†Corresponding author: bigot@unistra.fr

garnet over a broad temperature range in the vicinity of the magnetization compensation point. We demonstrate that the heat energy provided by exciting the phonon-assisted d-d transitions is efficient to induce an ultrafast magnetization dynamics with large amplitude at a temperature slightly below the magnetization compensation point of a ferrimagnetic insulator. Furthermore, we find that this dynamics has unusual characteristics: It emerges several tens of picoseconds after the excitation and has long characteristic time of several hundreds of picoseconds. This relatively slow dynamics can be understood by considering the weak phonon-spin coupling in magnetic garnets.

The following is organized in three sections. First, we briefly describe in Sec. II the experimental details including the static magnetic and magneto-optical properties of the sample and the low-temperature pump-probe setup. In Sec. III we present and discuss the results of the study of the laser-induced ultrafast magnetization dynamics as a function of the temperature, the absorbed laser energy density E_{pump}, and the external magnetic field H_{ext}. In Sec. IV we summarize our findings.

II. SAMPLE PROPERTIES AND EXPERIMENTAL METHODS

Rare-earth iron garnets $Re_3Fe_5O_{12}$ are ferrimagnetic insulators with high Curie temperature ($T_C \sim 560$ K) and large band gap ($E_g \sim 2.3$ eV) [35,36]. They belong to the $Ia3d$ cubic space group where the magnetic ions are distributed over three crystallographic sites (tetrahedral $24d$, octahedral $16a$, and dodecahedral $24c$). The iron ions occupy the two nonequivalent tetrahedral and octahedral sites, which are coupled by a strong antiferromagnetic superexchange. The noncompensated iron magnetization (M_{Fe}) is coupled antiparallel to the rare-earth magnetization (M_{RE}) in the dodecahedral site. The different temperature dependences of M_{RE} and M_{Fe} lead to the appearance of the compensation temperature (T_M), where the net magnetization (M_s) vanishes. For the temperature below T_M, M_s is aligned in the direction of M_{RE}, while above T_M, M_s aligns in the direction of M_{Fe}.

The experiments were performed on 7-μm-thick $(GdTmPrBi)_3(FeGa)_5O_{12}$ single crystalline garnet film, grown by liquid phase epitaxy on gadolinium gallium garnet (GGG) (111) substrate. The magnetization of the dodecahedral sublattices arises mainly from the Gd ions, where a very small amount of Pr is used to increase the uniaxial magnetic anisotropy [37]. The nonmagnetic elements in the chemical formula are added to improve specific properties of the sample such as the magneto-optical response and the optical transparency. The Tm and Bi ions in dodecahedral sites allow, respectively, compensation of the lattice mismatch with the substrate and increase of the magneto-optical response. The Ga dilutes both iron sublattices with a strong preference for tetrahedral sites, which allows for improving the transparency of the sample and controlling the value of T_C [36].

The static magnetic and magneto-optical (MO) properties of the film are characterized by the MO Kerr effect, using a homemade magnetometer setup based on modulation polarization technique [25,38]. The polar hysteresis loops measured as a function of temperature with an external magnetic field applied perpendicular to the film plane are shown in
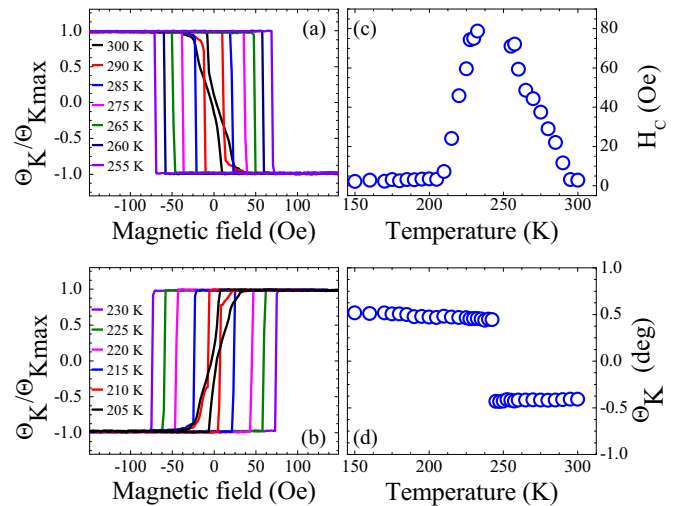

FIG. 1. Static magneto-optical properties of the garnet film as a function of temperature. (a, b) Normalized polar Kerr hysteresis loops measured over a broad temperature range above (a) and below (b) the compensation temperature T_M. (c, d) Temperature dependence of the coercive field H_C and the polar Kerr rotation Θ_K measured at the photon energy 3.1 eV.

Figs. 1(a) and 1(b), respectively, by the normalized Kerr rotation Θ_K. The loops have a perfect square shape in the temperature range from 210 to 290 K, revealing a uniaxial magnetic anisotropy perpendicular to the film plane. Outside of this temperature range, the hysteresis loops are not square, as can be seen at 300 and 205 K. This is due to the small size of the magnetic domains ($\sim 10\ \mu$m^2) compared to the light spot size in the static MO setup (~ 1 mm^2). To further highlight the temperature dependence of the magnetic and MO properties, the temperature dependence of the coercive field H_C and the amplitude of Θ_K are presented in Figs. 1(c) and 1(d), respectively. H_C has a clear divergence near 245 ± 5 K, which is the T_M of the film. Furthermore, at the temperature T_M, Θ_K changes sign, whereas its absolute value is almost constant. This behavior is in agreement with the approach that describes the MO effects in Bi-doped iron garnet by diamagnetic transitions associated to the crystal field energy-level diagram of iron atoms in tetrahedral and octahedral sublattices [38,39]. It also reveals that M_{Fe} is almost constant between 150 and 300 K, and, therefore, the high-temperature dependence of M_{Gd} in this temperature range leads to the ferrimagnetic compensation point [36,40].

The laser-induced ultrafast magnetization dynamics was investigated by time-resolved magneto-optical Kerr effect (TR-MOKE) using the pump-probe configuration sketched in the inset of Fig. 2(a). The pump and probe beams are generated from the output of an amplified Ti:sapphire laser system operating at a 5-kHz repetition rate and delivering 50-fs pulses at 1.55 eV. The pump beam is kept at the fundamental of the amplifier at 1.55 eV. This pump photon energy is below the band gap, which allows a homogeneous excitation over the entire depth of the sample. The probe is frequency doubled with a nonlinear barium boron oxide crystal. At the probe photon energy (3.1 eV), the MO signal comes from the Fe^{3+} spins and only the first 540 ± 50 nm of the sample are probed. This value
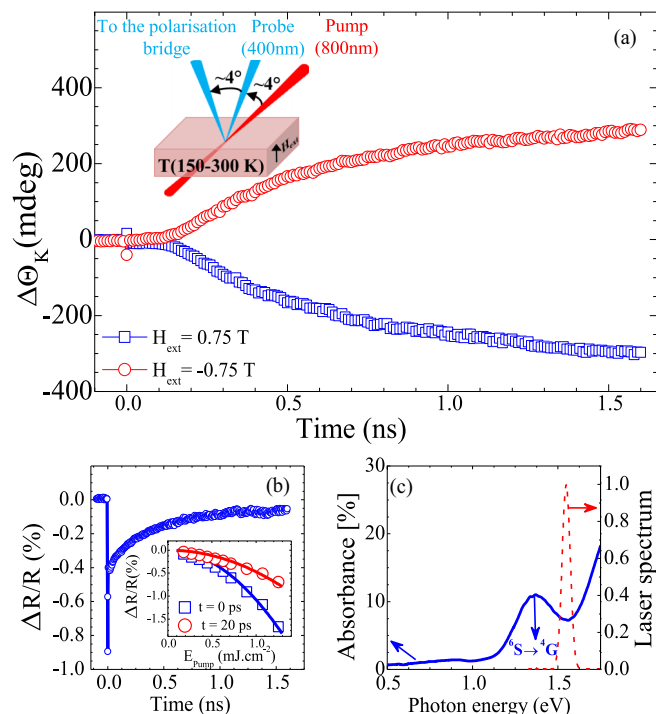
FIG. 2. Laser-induced magnetization dynamics in the garnet film. (a, b) $\Delta\Theta_K$ and $\Delta R/R$ induced by an absorbed energy density of $0.89 \, \text{mJ cm}^{-2}$ for $H_{\text{ext}} = \pm 0.75 \, \text{T}$ and at a temperature of 240 K. (c) The optical absorption spectra of the sample at 300 K, including the laser pulse spectrum and the d-d transition associated to the peak at 1.38 eV. Insets: (a) Sketch of the TR-MOKE configuration and (b) $\Delta R/R$ measured at two different time delays of 0 and 20 ps as a function of the pump energy density. The solid lines are the fits to the data using $\Delta R/R = b(E_{\text{pump}})^2$.

is obtained from optical studies performed in transmission geometry on comparable samples with lower thicknesses. The angles of incidence for the pump and probe beams were $2°$ and $6°$, respectively. Both beams are linearly polarized and focused onto the sample in spot diameters of $\sim 150 \, \mu$m for the pump and $\sim 60 \, \mu$m for the probe. The sample is mounted in a helium-cooled cryostat with temperature stability better than 0.2 K. The external magnetic field H_{ext} is applied perpendicular to the film plane and its magnitude is larger than H_C, ensuring the same magnetic state for each exiting pump pulse. The differential change of the normalized differential reflectivity $\Delta R/R(t)$ and the absolute differential Kerr rotation $\Delta\Theta_K(t)$ induced by the pump beam are simultaneously measured as a function of the delay "t" between the pump and the probe using a polarization bridge and a synchronous detection technique.

III. RESULTS AND DISCUSSION

Figure 2(a) displays the TR-MOKE measurement of the magnetization dynamics induced by an absorbed pump energy density of $0.89 \, \text{mJ cm}^{-2}$ at a temperature of 240 K and for $H_{\text{ext}} = 0.75 \, \text{T}$. Two important features can be clearly distinguished. First, the $\Delta\Theta_K$ signal measured during the first ~ 100 ps after the excitation is very weak (less than 1%) for both directions of the field. Second, a gradual change of the

$\Delta\Theta_K$ signal starts at ~ 100 ps and reaches a large values at 1.6 ns. Let us mention that the change of sign of $\Delta\Theta_K$ when the direction of the magnetic field is reversed demonstrates the magnetic origin of the signal. The decrease of magnetization ($[\Delta\Theta_K]^{H+} - [\Delta\Theta_K]^{H-}$) occurs with a characteristic time of 445 ± 30 ps. We also note that we have found that the signal $\Delta\Theta_K$ is independent on the pump polarization state (not shown), indicating the thermal origin of the excitation. The pump-induced change in the reflectivity signal $\Delta R/R(t)$ is displayed in Fig. 2(b). During the overlap between the pump and probe, a large peak is observed. After this peak, the residual $\Delta R/R$ signal shows a relaxation process with a characteristic time of 377 ± 6 ps.

The observed magnetization dynamics is related to the heat induced by the pump pulse. It is therefore important to understand the heating process in the magnetic garnets to explain the observed behavior. For this reason, we measured the absorption spectrum of the studied film [Fig. 2(c)]. Near the pump photon energy, there is a weak broad absorption band related to the d-d transition between the ground state $^6A_{1g}$ (^6S) and the first excited state $^4T_{1g}$ (^4G) of Fe^{3+} ions in octahedral sites [41]. We note that the absorption coefficient of this d-d transition is of $\sim 150 \, \text{cm}^{-1}$, which is very small compared to the one associated with the charge-transfer transitions ($\sim 10^5 \, \text{cm}^{-1}$) that define the energy band gap in iron garnets [41]. In Fig. 2(c) it corresponds to the very large onset of absorption for our relatively thick sample (7 μm). The d-d transition is formally electric-dipole forbidden per parity and spin selection rules. However, due to the spin-orbit coupling and the phonon-assisted transitions process, the selection rules are lifted with a corresponding moderate absorption coefficient in many oxides [42,43]. The phonons created during the excitation of the d-d transitions are associated with an ultrafast heating of the lattice within hundreds of femtoseconds [44]. It is a linear process with respect to the pump energy density. On the other hand, we mention that the peaks observed in $\Delta\Theta_K$ and ΔR at the zero time delay can be a result of the population of the excited state in the Fe^{3+} ion at the probe photon energy by the two-photon absorption process. It is expected to be quadratic with respect to the pump energy density. Therefore, we investigated the variation of $\Delta R/R$ as a function of the pump energy density at two different time delays of 0 and 20 ps as shown in the inset of Fig. 2(b). The data can be fitted by $\Delta R/R = b(E_{\text{pump}})^2$, revealing the existence of a two-photon absorption process. This is in agreement with previous finding in iron garnet excited with pump photon energy at 1.55 eV [27]. The two-photon absorption can be related to the d-d transition between the ground state $^6A_{1g}$ (^6S) and the second excited state $^4T_{1g}$ (^4P) of Fe^{3+} ions in octahedral sites, which is predicted at ~ 3.11 eV for iron garnet films with low bismuth concentration ($x_{\text{Bi}} < 1$) [36,45–47] as it is the case for our sample. This transition also leads to an ultrafast heating of the lattice. The TR-MOKE signal is thus due to the transfer of the heat energy from the hot lattice to the spins, which occurs via the phonon-magnon coupling. The overall process involves both a direct excitation of phonons (d-d transitions $^6S \rightarrow {}^4G$) and a secondary excitation of phonons via the two-photon transitions ($^6S \rightarrow {}^4P$).

Owing to the presence of different magnetics sublattices, three different effects related to the heat transfer from the lattice to the spins can be distinguished in the studied garnet film. The
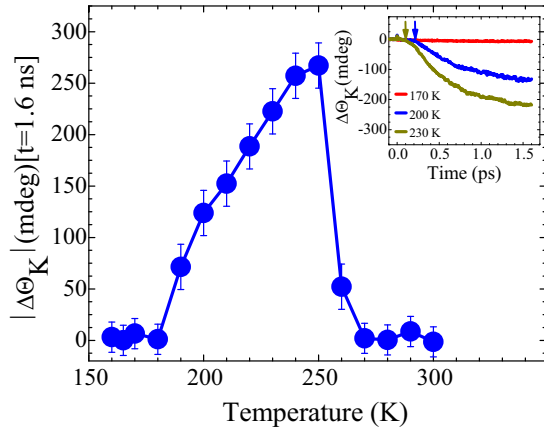
FIG. 3. Temperature dependence of laser-induced magnetization dynamics. The absolute value of the amplitude $\Delta\Theta_K$ ($t = 1.6$ ns) as a function of the temperature. The inset shows $\Delta\Theta_K$ measured at selected temperatures below T_M. All measurements are obtained for a pump energy density $E_{\text{pump}} = 1.34$ mJ cm^{-2} and $H_{\text{ext}} = 0.5$ T.

first is a demagnetization of the Fe^{3+} sublattices. This effect cannot be at the origin of the very large signal observed in the TR-MOKE for the time delay larger than $\sim$100 ps. This is because M_{Fe} is almost constant over a large temperature range above 240 K which cannot be exceeded by the amount of a few tens of kelvins associated with a heating process typically induced by exciting d-d transitions [32,33,44]. The second effect is a demagnetization of the Gd sublattice, which can be very large as M_{Gd} strongly depends on the temperature near T_M [36,40]. Such an effect, however, should start immediately after the optical excitation. In addition, it cannot be directly detected with a MO signal coming from the Fe^{3+} sublattices. The third effect is a reversal process of the M_{Fe} toward the direction of the magnetic field, which occurs when M_{Fe} becomes larger than M_{Gd}. This behavior is qualitatively in agreement with the TR-MOKE results. Indeed, the delay of $\sim$100 ps for the onset of the magnetization reversal process can be explained by a very slow demagnetization time of M_{Gd} due to the weak phonon-magnon coupling characterizing the magnetic garnet [48–50]. To substantiate the proposed origin of the TR-MOKE signal we performed measurements at different sample temperatures. Let us mention that in the rest of the paper we define $\Delta\Theta_K$ as $([\Delta\Theta_K]^{H+} - [\Delta\Theta_K]^{H-})/2$. The temperature dependence of the absolute value of $\Delta\Theta_K$ ($t = 1.6$ ns) is shown in Fig. 3. The signal vanishes in the temperature range below 190 K where M_{Gd} is highly sensitive to the changes of temperature caused by the pump pulse. This clearly establishes that the probe photon energy is only sensitive to the Fe^{3+} sublattices. On the other hand, the weak signals measured above T_M confirm that the magnetization dynamics observed below T_M is related to the magnetization reversal process of M_{Fe}. We also find that the magnetization reversal dynamics can be observed from the temperature of 190 K and the maximum of the effect is obtained at T_M. Importantly the starting time of the reversal processes decreases when the temperature increases from 190 K to T_M [see inset in Fig. 3(a)]. This behavior highlights the crucial role played by the initial value of M_{Gd} and its demagnetization at the onset of the reversal process.
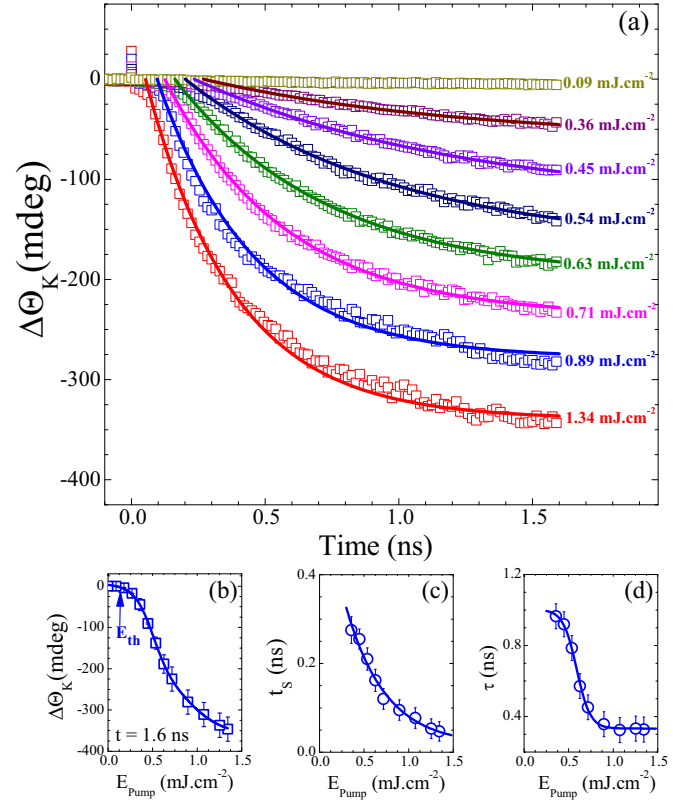

FIG. 4. Pump energy density dependence of the magnetization dynamics. (a) $\Delta\Theta_K$ measured at different pump energy densities. The solid lines are the fits using Eq. (1). (b–d) Pump energy density dependence of (b) the amplitude $\Delta\Theta_K$ ($t = 1.6$ ns) and (c, d) the elapses time t_s and characteristic time τ of the magnetization reversal dynamics. The inset shows $\Delta\Theta_K$ in logarithmic scale. The solid lines in the inset and (b–d) are guides to the eyes. All measurements are obtained at the temperature 240 K and for $H_{\text{ext}} = 1$ T.

To study the light-induced thermal magnetization reversal process in more detail, we have investigated the magnetization dynamics as a function of the pump energy density E_{pump}. TR-MOKE measurements at selected E_{pump} are displayed in Fig. 4(a). At low pump energy density ($E_{\text{pump}} = 0.09$ mJ cm^{-2}), the TR-MOKE signal is not affected by the optical excitation. This indicates that M_{Gd} is still larger than M_{Fe} 1.6 ns after the excitation, and therefore the magnetization reversal dynamic does not occur yet. The magnetization reversal dynamics is observed for $E_{\text{pump}} = 0.36$ mJ cm^{-2} and by further increasing E_{pump} it becomes more and more pronounced. We also note that the elapse time of the magnetization reversal process continuously decreases when increasing E_{pump}. To compare more precisely the characteristics of the magnetization reversal dynamics, TR-MOKE signals are fitted with the following function:

$$\Delta\Theta_K(t \geqslant t_S) = [A(1 - e^{-(t-t_S)/\tau})]H(t - t_s), \qquad (1)$$

where A is the maximum amplitude of the signal in the explored time scale, i.e., $A = \Delta\Theta_K$ ($t = 1.6$ ns); t_S is the elapsed time of the magnetization reversal process; τ represents the characteristic rise time of the magnetization reversal process; and $H(t - t_s)$ is a Heaviside function. Equation (1)
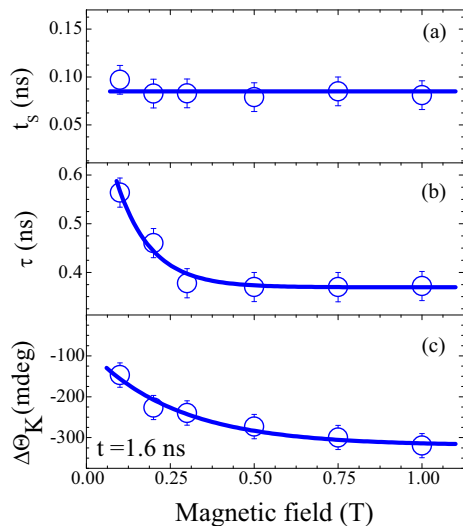
FIG. 5. Magnetic field dependence of laser-induced magnetization dynamics. (a, b) Variation of the elapsed time t_s and the characteristic time τ of the magnetization reversal dynamics as a function of H_{ext}. (c) Field dependence of the amplitude $\Delta\Theta_K$ ($t = 1.6$ ns). All measurements are obtained at the temperature 240 K and for $E_{pump} = 1.07$ mJ cm^{-2}.

is phenomenological, based on observations, and does not rely on a specific theoretical model. The corresponding fitting with Eq. (1) is plotted in Fig. 4(a) with solid lines showing a good agreement with the experimental data. Figures 4(b)–4(d) display the values of $\Delta\Theta_K$ ($t = 1.6$ ns), t_S, and τ as a function of E_{pump}. The behavior of $\Delta\Theta_K$ ($t = 1.6$ ns) reveals a threshold energy density $E_{th} \approx 0.15$ mJ cm^{-2} for the occurrence of the magnetization reversal dynamics during the first 1.6 ns after the excitation [see Fig. 4(b)]. Furthermore, we show that the characteristic times of the magnetization reversal dynamics t_S and τ decrease strongly with increasing E_{pump} [see Figs. 4(c) and 4(d)]. These features clearly demonstrate that the speed and the amplitude of the magnetization reversal dynamics can be controlled by varying the laser energy density. Let us note that the modification of t_S as a function of E_{pump} can be explained by an increase of the demagnetization speed of M_{Gd} when E_{pump} increases. The criterion that M_{Fe} is slightly larger than M_{Gd}, which is necessary for the occurrence of the magnetization reversal dynamics, is therefore satisfied at short delays. On the other hand, let us mention that the different behavior of $\Delta\Theta_K$ ($t = 1.6$ ns) and τ at high E_{pump} shows the relative simplicity of Eq. (1) compared to the complex magnetization reversal dynamics across T_M. Indeed, in addition to the coherent magnetization dynamics toward H_{ext}, the nucleation and domain-wall motion can play a role in the reversal process [18].

To further investigate the reversal dynamics, we studied the magnetic field dependence of the TR-MOKE signal. The extracted results after analyzing the data with Eq. (1) are

presented in Fig. 5. The elapsed time of the reversal dynamics is independent of the field [see Fig. 5(a)]. This is in agreement with our above prediction suggesting that t_s is related to the demagnetization of M_{Gd} until it becomes smaller than M_{Fe}, since the demagnetization process is also independent of the field. On the other hand, when increasing the field τ decreases while the $\Delta\Theta_K$ ($t = 1.6$ ns) increases [see Figs. 5(b) and 5(c)]. These two behaviors indicate a speedup of the reversal dynamics when the field becomes larger, which is the expected behavior for a magnetization reversal dynamics across T_M [17,18] as shown in metallic GdFeCo ferromagnetic films. Indeed, the time required to align the magnetization toward the field direction first decreases for moderate fields ($H < 0.25$ T) and then tends to saturate for larger fields. Let us mention that the speedup of the reversal dynamics when increasing the pump energy density is also in agreement with the results obtained in metallic ferrimagnets [17]. The main difference between the reversal dynamics across T_M in dielectric and metallic ferrimagnets is the onset time of the underlying process, which occurs at shorter time in metallic ferrimagnets. This can be attributed to the strong electron spin coupling in metallic ferrimagnets compared to the magnon-phonon coupling in iron garnets.

IV. CONCLUSIONS

We demonstrate that femtosecond laser pulses can induce a large-amplitude magnetization dynamics at temperature slightly below T_M of a ferrimagnetic insulator. This effect, shown here in Bi-doped gadolinium iron garnet, is caused by the heat energy produced by exciting the $^6S \rightarrow {}^4G$ and $^6S \rightarrow {}^4P$ phonon-assisted d-d transitions simultaneously by one- and two-photon absorption processes, and transferred to the spin system via the spin-lattice interaction. By tuning the laser energy density or the amplitude of the external magnetic field, the speed and the amplitude of the magnetization dynamics can be controlled. For large laser energy densities, we observe that this dynamics occurs ~50 ps after the excitation. The origin of this long delay between the excitation and the beginning of the magnetization dynamics arises from the slow demagnetization of the localized moment of the Gd sublattice due to the weak spin-lattice interaction in magnetic garnets. Moreover, we provide a detailed quantitative analysis of the amplitude and characteristic times (delay t_S and demagnetization time τ) of the magnetization dynamics as a function of either the laser energy density E_{pump} or the external magnetic field H_{ext}. The results are found to be in qualitative agreement with a magnetization reversal dynamics when approaching the compensation temperature T_M.

[1] G. Zhang, W. Hübner, E. Beaurepaire, and J.-Y. Bigot, in *Spin Dynamics in Confined Magnetic Structures I*, edited by B. Hillebrands and K. Ounadjela (Springer, Berlin, 2002), p. 245.

[2] U. Bovensiepen, Nat. Phys. **5**, 461 (2009).

[3] E. Beaurepaire, J. C. Merle, A. Daunois, and J. Y. Bigot, Phys. Rev. Lett. **76**, 4250 (1996).

[4] J. Y. Bigot, M. Vomir, L. H. F. Andrade, and E. Beaurepaire, Chem. Phys. **318**, 137 (2005).

[5] M. van Kampen, C. Jozsa, J. T. Kohlhepp, P. LeClair, L. Lagae, W. J. M. de Jonge, and B. Koopmans, Phys. Rev. Lett. **88**, 227201 (2002).

[6] A. V. Kimel, A. Kirilyuk, P. A. Usachev, R. V. Pisarev, A. M. Balbashov, and T. Rasing, Nature (London) **435**, 655 (2005).

[7] C. D. Stanciu, F. Hansteen, A. V. Kimel, A. Kirilyuk, A. Tsukamoto, A. Itoh, and T. Rasing, Phys. Rev. Lett. **99**, 047601 (2007) .

[8] S. Mangin *et al.*, Nat. Mater. **13**, 286 (2014).

[9] E. Beaurepaire, M. Maret, V. Halté, J. C. Merle, A. Daunois, and J. Y. Bigot, Phys. Rev. B **58**, 12134 (1998).

[10] G. Ju, J. Hohlfeld, B. Bergman, R. J. M. van de Veerdonk, O. N. Mryasov, J.-Y. Kim, X. Wu, D. Weller, and B. Koopmans, Phys. Rev. Lett. **93**, 197403 (2004).

[11] J. A. de Jong, I. Razdolski, A. M. Kalashnikova, R. V. Pisarev, A. M. Balbashov, A. Kirilyuk, T. Rasing, and A. V. Kimel, Phys. Rev. Lett. **108**, 157601 (2012).

[12] A. Alekhin *et al.*, Phys. Rev. Lett. **119**, 017202 (2017).

[13] G.-M. Choi, B.-C. Min, K.-J. Lee, and D. G. Cahill, Nat. Commun. **5**, 4334 (2014).

[14] J.-Y. Bigot, M. Vomir, and E. Beaurepaire, Nat. Phys. **5**, 515 (2009).

[15] K. Vahaplar, A. M. Kalashnikova, A. V. Kimel, D. Hinzke, U. Nowak, R. Chantrell, A. Tsukamoto, A. Itoh, A. Kirilyuk, and Th. Rasing, Phys. Rev. Lett. **103**, 117201 (2009).

[16] T. A. Ostler *et al.*, Nat. Commun. **3**, 666 (2012).

[17] C. D. Stanciu, A. Tsukamoto, A. V. Kimel, F. Hansteen, A. Kirilyuk, A. Itoh, and T. Rasing, Phys. Rev. Lett. **99**, 217204 (2007).

[18] Z. Chen, R. Gao, Z. Wang, C. Xu, D. Chen, and T. Lai, J. Appl. Phys. **108**, 023902 (2010).

[19] I. Radu *et al.*, Nature (London) **472**, 205 (2011).

[20] G.-M. Choi, A. Schleife, and D. G. Cahill, Nat. Commun. **8**, 15085 (2017).

[21] A. M. Kalashnikova, A. V. Kimel, R. V. Pisarev, V. N. Gridnev, A. Kirilyuk, and T. Rasing, Phys. Rev. Lett. **99**, 167205 (2007).

[22] F. Hansteen, A. Kimel, A. Kirilyuk, and T. Rasing, Phys. Rev. Lett. **95**, 047402 (2005).

[23] T. Satoh *et al.*, Phys. Rev. Lett. **105**, 077402 (2010).

[24] B. Koene, M. Deb, E. Popova, N. Keller, T. Rasing, and A. Kirilyuk, Phys. Rev. B **91**, 184415 (2015).

[25] M. Deb, M. Vomir, J.-L. Rehspringer, and J.-Y. Bigot, Appl. Phys. Lett. **107**, 252404 (2015).

[26] M. Deb, P. Molho, B. Barbara, and J.-Y. Bigot, Phys. Rev. B **94**, 054422 (2016).

[27] B. Koene, M. Deb, E. Popova, N. Keller, T. Rasing, and A. Kirilyuk, J. Phys.: Condens. Matter **28**, 276002 (2016).

[28] S. Parchenko, A. Stupakiewicz, I. Yoshimine, T. Satoh, and A. Maziewski, Appl. Phys. Lett. **103**, 172402 (2013).

[29] S. Parchenko, T. Satoh, I. Yoshimine, F. Stobiecki, A. Maziewski, and A. Stupakiewicz, Appl. Phys. Lett. **108**, 032404 (2016).

[30] M. V. Gerasimov, M. V. Logunov, A. V. Spirin, Y. N. Nozdrin, and I. D. Tokman, Phys. Rev. B **94**, 014434 (2016).

[31] A. F. Kabychenkov, Phys. Solid State **48**, 516 (2006).

[32] A. V. Kimel, C. D. Stanciu, P. A. Usachev, R. V. Pisarev, V. N. Gridnev, A. Kirilyuk, and T. Rasing, Phys. Rev. B **74**, 060403 (2006).

[33] J. A. de Jong, A. V. Kimel, R. V. Pisarev, A. Kirilyuk, and T. Rasing, Phys. Rev. B **84**, 104421 (2011).

[34] T. Tsuyama, S. Chakraverty, S. Macke, N. Pontius, C. Schüßler-Langeheine, H. Y. Hwang, Y. Tokura, and H. Wadati, Phys. Rev. Lett. **116**, 256402 (2016).

[35] G. D. Winkler, *Magnetic Garnets* (Vieweg, Braunschweig, 1981).

[36] G. F. Dionne, *Magnetic Oxides* (Springer, Berlin, 2009).

[37] P. Molho and M. P. de Albuquerque, J. Magn. Magn. Mater. **226–230**, 1388 (2001).

[38] M. Deb, E. Popova, A. Fouchet, and N. Keller, J. Phys. D Appl. Phys. **45**, 455001 (2012).

[39] G. F. Dionne and G. A. Allen, J. Appl. Phys. **75**, 6372 (1994).

[40] H. Miyagawa, N. Kawamura, and M. Suzuki, Phys. Scr. **2005**, 616 (2005).

[41] G. B. Scott, D. E. Lacklison, and J. L. Page, Phys. Rev. B **10**, 971 (1974).

[42] L. L. Lohr, Coordin. Chem. Rev. **8**, 241 (1972).

[43] P. Chen, N. Lee, S. McGill, S. W. Cheong, and J. L. Musfeldt, Phys. Rev. B **85**, 174413 (2012).

[44] A. V. Kimel, R. V. Pisarev, J. Hohlfeld, and T. Rasing, Phys. Rev. Lett. **89**, 287401 (2002).

[45] G. A. Allen and G. F. Dionne, J. Appl. Phys. **73**, 6130 (1993).

[46] L. E. Helseth, A. G. Solovyev, R. W. Hansen, E. I. Il'yashenko, M. Baziljevich, and T. H. Johansen, Phys. Rev. B **66**, 064405 (2002).

[47] L. E. Helseth, R. W. Hansen, E. I. Il'yashenko, M. Baziljevich, and T. H. Johansen, Phys. Rev. B **64**, 174406 (2001).

[48] G. F. Dionne and G. L. Fitch, J. Appl. Phys. **87**, 4963 (2000).

[49] E. G. Spencer and R. C. LeCraw, Phys. Rev. Lett. **4**, 130 (1960).

[50] D. L. Huber, Phys. Rev. **136**, A500 (1964).